Improved short-segment detection statistic for continuous gravitational waves

P. B. Covas* and R. Prix

Max Planck Institute for Gravitational Physics (Albert Einstein Institute), D-30167 Hannover, Germany

(Received 16 March 2022; accepted 20 May 2022; published 6 June 2022)

Continuous gravitational waves represent one of the long-sought types of signals that have yet to be detected. Due to their small amplitude, long observational datasets (months–years) have to be analyzed together, thereby vastly increasing the computational cost of these searches. All-sky searches face the most severe computational obstacles, especially searches for sources in unknown binary systems, which need to break the data into very short segments in order to be computationally feasible. In this paper, we present a new detection statistic that improves sensitivity by up to 19% compared to the standard $\mathcal{F}$-statistic for segments shorter than a few hours.

DOI: 10.1103/PhysRevD.105.124007

I. INTRODUCTION

Continuous gravitational waves (CWs) are long-lasting and nearly monochromatic signals, expected to be emitted by asymmetric rotating neutron stars [1,2]. While there have been many searches for CWs performed to date, none has yet been able to make a detection. One of the main difficulties in finding CWs is their small amplitude, expected to be many orders of magnitude below the noise floors of current detectors. In order to accumulate a detectable signal-to-noise ratio, large datasets (spanning months–years) therefore have to be combined in a search, which complicates the analysis and results in a vast increase in computing cost due to the astronomically large number of templates to be searched.

We can divide searches for CWs into three main categories, ordered by increasing computational cost: (i) targeted searches, (ii) directed searches, and (iii) all-sky searches. Directed and all-sky searches typically cannot combine all the data coherently due to the unfeasible computational cost this would entail and instead have to employ semicoherent algorithms by breaking the data into shorter segments (e.g., see [3,4]). Although the total signal power does not depend on the number of segments used, the background (i.e., noise) distribution worsens when the number of segments increases. Therefore, while using more segments dramatically alleviates the computational cost of the search, it also reduces the resulting sensitivity. The optimal search setup consists of using the longest segments possible within a given computational cost budget [4].

There are various ways to compute semicoherent detection statistics, but one widely used approach we focus on here consists in summing coherent $\mathcal{F}$-statistics [5,6] across segments, known as the *StackSlide* approach (see also [7] for more discussion and an overview of different methods currently in use). The corresponding $\mathcal{F}$-statistic segments used have so far always been longer than ∼11 h. At the other end of the spectrum are the "power" statistics, which directly use Fourier power over short segments, typically no longer than ∼1 h, as the per-segment statistic.

A recent search [8] has bridged this gap for the first time by employing a semicoherent $\mathcal{F}$-statistic on short segments of 900 s, designed to improve the sensitivity of an all-sky search for signals from unknown neutron stars in binary systems. Using the $\mathcal{F}$-statistic on such short segments has resulted in unexpected and previously unknown numerical difficulties, with the $\mathcal{F}$-statistic becoming singular in many segments, especially those containing data from only one detector. This degeneracy can be easily understood from the underlying antenna-pattern matrix becoming ill conditioned for short coherence times and the $\mathcal{F}$-statistic relying on inverting this matrix. Intuitively this corresponds to a failure of the maximum-likelihood estimation of the four unknown amplitude parameters (describing the "+" and "×" polarizations) for short coherence times, during which the detector hardly moves.

In an attempt to fix this singularity by constructing a well-behaved "fallback" statistic, we have discovered a new detection statistic that is not just well behaved in the short-segment limit but turns out to be *more sensitive* than

*pep.covas.vidal@aei.mpg.de

the $\mathcal{F}$-statistic for segments shorter than a few hours, even when the $\mathcal{F}$-statistic is far from numerically singular.

This paper is organized as follows: in Sec. II, we introduce the standard $\mathcal{F}$-statistic. Section III discusses the singular limit of the $\mathcal{F}$-statistic for short segments, and Sec. IV introduces the new statistic. Section IV characterizes the sensitivity improvement of the new statistic compared to the $\mathcal{F}$-statistic, and Sec. V provides numerical tests for these analytical results and further characterizes the new statistic, followed by conclusions in Sec. VI. The Appendix discusses an alternative short-segment statistic construction that turns out to be unsuitable for multidetector setups.

II. THE STANDARD $\mathcal{F}$-STATISTIC

A. The continuous-waves likelihood

We can parametrize the gravitational-wave signal from a nonaxisymmetric rotating neutron star by four amplitude parameters $\mathcal{A}$ and several phase-evolution parameters λ. The four amplitude parameters consist of the overall signal amplitude h_0, the inclination angle ι between the line of sight and the neutron star rotation axis, the phase ϕ_0 at a reference time, and a polarization angle ψ. The phase-evolution parameters consist of the frequency of the signal f (slowly changing over time), the sky position of the neutron star, and binary-orbital parameters if the neutron star is in a binary.

The CW signal depends nonlinearly on the physical amplitude parameters $\{h_0, \cos\iota, \psi, \phi_0\}$, but in [5], the authors found a set of four amplitude coordinates $\mathcal{A}^\mu$ that linearize the functional form of the signal, namely,

$$\begin{aligned}
\mathcal{A}^1 &= A_+ \cos\phi_0 \cos 2\psi - A_\times \sin\phi_0 \sin 2\psi,\\
\mathcal{A}^2 &= A_+ \cos\phi_0 \sin 2\psi + A_\times \sin\phi_0 \cos 2\psi,\\
\mathcal{A}^3 &= -A_+ \sin\phi_0 \cos 2\psi - A_\times \cos\phi_0 \sin 2\psi,\\
\mathcal{A}^4 &= -A_+ \sin\phi_0 \sin 2\psi + A_\times \cos\phi_0 \cos 2\psi,
\end{aligned} \tag{1}$$

where $A_+ = 0.5h_0(1+\cos^2\iota)$ and $A_\times = h_0\cos\iota$ are the amplitudes of the "+" and "×" polarization, respectively. This allows one to write a signal $s^X(t)$ in the frame of detector X as

$$s^X(t;\mathcal{A},\lambda) = \sum_{\mu=1}^{4} \mathcal{A}^\mu h_\mu^X(t;\lambda), \tag{2}$$

where the matched-filter basis functions are defined as

$$\begin{aligned}
h_1^X &\equiv a^X(t)\cos\phi^X(t), \qquad h_2^X \equiv b^X(t)\cos\phi^X(t),\\
h_3^X &\equiv a^X(t)\sin\phi^X(t), \qquad h_4^X \equiv b^X(t)\sin\phi^X(t),
\end{aligned} \tag{3}$$

in terms of the detector-frame signal phase $\phi^X(t)$ at time t and the antenna-pattern functions $a^X(t)$ and $b^X(t)$ [5,9].

A detection statistic typically aims to distinguish two basic hypotheses about the data $x(t)$: (i) the data only consist of Gaussian noise n, i.e., $x = n$, or (ii) the data consist of an astrophysical signal s in addition to Gaussian noise, i.e., $x = n + s$. The likelihood ratio $\mathcal{L}$ between these two hypothesis is

$$\begin{aligned}
\ln\mathcal{L}(x;\mathcal{A},\lambda) &\equiv \ln\frac{P(x|\text{signal})}{P(x|\text{noise})} = (x|h) - \frac{1}{2}(h|h)\\
&= \mathcal{A}^\mu x_\mu - \frac{1}{2}\mathcal{A}^\mu \mathcal{M}_{\mu\nu}\mathcal{A}^\nu,
\end{aligned} \tag{4}$$

with implicit summation over $\mu,\nu = 1,\ldots,4$ and where we defined

$$x_\mu \equiv (x|h_\mu), \qquad \mathcal{M}_{\mu\nu} \equiv (h_\mu|h_\nu), \tag{5}$$

in terms of the multidetector scalar product[1] [6,9]

$$(x|y) \equiv 2\mathcal{S}^{-1}\sum_X^{N_{\text{det}}}\sqrt{w_X}\int_0^T x^X(t)y^X(t)dt, \tag{6}$$

where $\mathcal{S}$ represents the overall noise floor, defined as

$$\mathcal{S}^{-1} \equiv \frac{1}{N_{\text{det}}}\sum_X S_X^{-1}, \tag{7}$$

and w_X is a per-detector noise weight defined as

$$w_X \equiv \frac{S_X^{-1}}{\mathcal{S}^{-1}}. \tag{8}$$

For ease of notation, here we assume stationary noise floors S_X for each detector X, while the numerical implementation [9,10] uses a more general formulation valid also for slowly varying noise floors.

The antenna-pattern matrix $\mathcal{M}_{\mu\nu}$ defined in Eq. (5) can be expressed more explicitly as

$$\mathcal{M}_{\mu\nu} = \gamma\begin{pmatrix} A & C & 0 & 0\\ C & B & 0 & 0\\ 0 & 0 & A & C\\ 0 & 0 & C & B\end{pmatrix}, \tag{9}$$

with the "data factor" γ defined as

$$\gamma \equiv \mathcal{S}^{-1}T_{\text{data}}, \tag{10}$$

where T_{data} is the total amount of data over all detectors (e.g., $T_{\text{data}} = N_{\text{det}}T$ if there are no data gaps) and the sky-position dependent antenna-pattern coefficients

[1]For simplicity of notation, here we assume stationary noise and contiguous data T, see [9] for a more general expression.

$$A \equiv \langle \boldsymbol{a}^2 \rangle, \qquad B \equiv \langle \boldsymbol{b}^2 \rangle, \qquad C \equiv \langle \boldsymbol{a}\boldsymbol{b} \rangle, \tag{11}$$

using the noise-weighted multidetector time average

$$\langle \boldsymbol{Q} \rangle \equiv \frac{1}{N_{\mathrm{det}}} \sum_X^{N_{\mathrm{det}}} \sqrt{w_X} \langle Q^X \rangle, \quad \text{with}$$
$$\langle Q^X \rangle \equiv \frac{1}{T} \int_0^T Q^X(t) dt. \tag{12}$$

We define the block determinant D of $\mathcal{M}$ as

$$D \equiv AB - C^2, \tag{13}$$

such that $\det \mathcal{M} = D^2$. Note that the $x_\mu = n_\mu + s_\mu$ in Eq. (5) are Gaussian distributed with expectation and second moment

$$E[x_\mu] = s_\mu, \qquad E[x_\mu x_\nu] = \mathcal{M}_{\mu\nu} + s_\mu s_\nu. \tag{14}$$

B. The coherent $\mathcal{F}$-statistic

The likelihood ratio in Eq. (4) can be analytically maximized over the four amplitude coordinates $\mathcal{A}^\mu$, yielding the maximum-likelihood estimates

$$\mathcal{A}'^\mu = \mathcal{M}^{\mu\nu} x_\nu, \tag{15}$$

where $\mathcal{M}^{\mu\nu}$ is the inverse of the antenna-pattern matrix. Substituting back into Eq. (4) defines the $\mathcal{F}$-statistic as

$$2\mathcal{F}(x;\lambda) \equiv \ln \mathcal{L}(x;\lambda;\mathcal{A}') = x_\mu \mathcal{M}^{\mu\nu} x_\nu. \tag{16}$$

It is useful to write this out more explicitly in terms of the antenna-pattern-matrix elements of Eq. (9) as

$$2\mathcal{F} = \frac{(x_1^2 + x_3^2)B + (x_2^2 + x_4^2)A - 2(x_1 x_2 + x_3 x_4)C}{\gamma D}. \tag{17}$$

An alternative derivation of the $\mathcal{F}$-statistic as a Bayes factor [11] reveals the underlying amplitude priors to be unphysical, which is why the $\mathcal{F}$-statistic is not statistically optimal. The main advantage of the $\mathcal{F}$-statistic is the analytical elimination of the four amplitude parameters, which gives it a computational advantage over any alternative that would require explicit numerical operations to deal with the unknown amplitude parameters (e.g., see [12–14] for further discussion).

Another useful property of the $\mathcal{F}$-statistic is its known χ^2 probability distribution with $\nu = 4$ degrees of freedom and noncentrality parameter

$$\rho^2 \equiv (s|s) = \mathcal{A}^\mu \mathcal{M}_{\mu\nu} \mathcal{A}^\nu. \tag{18}$$

The known mean and variance of this distribution are

$$E[2\mathcal{F}] = \nu + \rho^2,$$
$$\mathrm{var}[2\mathcal{F}] = 2(\nu + 2\rho^2). \tag{19}$$

It will be useful to express the noncentrality as

$$\rho^2 = h_0^2 \gamma (\alpha_1 A + \alpha_2 B + 2\alpha_3 C), \tag{20}$$

in terms of amplitude angle factors $\alpha_i(\cos\iota, \psi)$ defined as

$$\alpha_1 \equiv \frac{1}{4}(1 + \cos^2\iota)^2 \cos^2 2\psi + \cos^2\iota \sin^2 2\psi,$$
$$\alpha_2 \equiv \frac{1}{4}(1 + \cos^2\iota)^2 \sin^2 2\psi + \cos^2\iota \cos^2 2\psi,$$
$$\alpha_3 \equiv \frac{1}{4}(1 - \cos^2\iota)^2 \sin 2\psi \cos 2\psi. \tag{21}$$

One can see that averaging over the unknown $\cos\iota$ and ψ yields $\langle \alpha_1 \rangle_{\cos\iota,\psi} = \langle \alpha_2 \rangle_{\cos\iota,\psi} = 2/5$ and $\langle \alpha_3 \rangle_{\cos\iota,\psi} = 0$, and therefore, the angle-averaged noncentrality parameter can be found as

$$\langle \rho^2 \rangle_{\cos\iota,\psi} = \frac{2}{5} h_0^2 \gamma (A + B). \tag{22}$$

C. The semicoherent $\hat{\mathcal{F}}$-statistic

The use of the coherent $\mathcal{F}$-statistic as a search method is practically limited to very small parameter spaces, due to the rapidly growing computing cost of a coherent template bank with increasing observation times T. Wide-parameter-space searches therefore have to employ cheaper *semicoherent* methods, which typically result in better sensitivity at constrained computing cost [3]. In the following, we focus on the semicoherent version of the $\mathcal{F}$-statistic.

We can break the total observation time T into $\ell = 1, \ldots, N_{\mathrm{seg}}$ *segments* of duration T_{seg} and define the semicoherent $\hat{\mathcal{F}}$-statistic as

$$\hat{\mathcal{F}} \equiv \sum_{\ell=1}^{N_{\mathrm{seg}}} \mathcal{F}_\ell, \tag{23}$$

where $\mathcal{F}_\ell$ is the coherent $\mathcal{F}$-statistic computed on segment ℓ. Because this is a sum of χ^2-distributed statistics, the semicoherent $\hat{\mathcal{F}}$-statistic is also χ^2 distributed, with $\hat{\nu}$ degrees of freedom and noncentrality parameter $\hat{\rho}^2$, given by

$$\hat{\nu} = \sum_\ell \nu_\ell = 4N_{\mathrm{seg}},$$
$$\hat{\rho}^2 = \sum_\ell \rho_\ell^2. \tag{24}$$

The optimal choice for the number and length of segments is subject to a computing-cost-constrained optimization

problem [4,15,16], but the general trend is that the larger the parameter space is, the shorter the segments must be in order for the search to be computationally feasible.

For example, a recent all-sky search for continuous waves from neutron stars in unknown binary systems [8] had to use very short segments of $T_{\mathrm{seg}} = 900$ s over an observation time of $T = 6$ months. This has revealed previously unknown problems and limitations of the $\mathcal{F}$-statistic over such short baselines, discussed in the next section.

III. PROBLEMS WITH SHORT-SEGMENT $\mathcal{F}$

A. The ill-conditioned short-segment limit

The $\mathcal{F}$-statistic relies on the inverse antenna-pattern matrix $\mathcal{M}^{\mu\nu}$, as seen in Eq. (16). However, for a single detector the short-duration limit of the matrix coefficients A, B, and C of Eq. (11) is

$$\{A, B, C\} \overset{T_{\mathrm{seg}}\to 0}{\to} \{a^2, b^2, ab\}, \tag{25}$$

which leads to a singular antenna-pattern matrix with determinant $\det \mathcal{M} = D^2 = (AB - C^2)^2 \to 0$. For short segments, the matrix therefore becomes ill conditioned, and computing D is unreliable or fails. For performance reasons the *lalsuite* [17] codes computing the $\mathcal{F}$-statistic use single precision for the antenna-pattern matrix, and computing D can therefore become problematic already at condition numbers above $\mathrm{cond}[\mathcal{M}] \gtrsim 10^4$, for which the code will refuse to compute a result.

The problem for single-detector segments is illustrated in Fig. 1: the left plot shows the block determinant D and the critical condition-number contour $\mathrm{cond}[\mathcal{M}] = 10^4$ over the sky for a single segment of $T_{\mathrm{seg}} = 900$ s. The right plot shows the fraction of segments with a supercritical condition number over the sky. We see that near the equator ~40% of the segments would be ill conditioned.

Combining data from more than one detector generally alleviates this problem, as C now tends to $\propto (\sum_X a^X)(\sum_Y b^Y)$, where the cross terms generally prevent the determinant from vanishing even when $T \to 0$. In practice, however, due to commonly found gaps in the detector data, a realistic segment setup with $T_{\mathrm{seg}} = 900$ s segments for two detectors (H1 + L1) (such as [8]) will contain many segments containing data from only one detector. Therefore, computing the $\mathcal{F}$-statistic on such segments will still encounter numerical problems.

Dropping such segments would reduce the amount of usable data and therefore sacrifice sensitivity (e.g., for the O3a LIGO science run, this affects about a *third* of such short segments [8]). This problem has motivated an investigation into a nonsingular "fallback" option for the singular $\mathcal{F}$-statistic on short segments.

B. Fallback construction for singular $\mathcal{F}$-statistic

As discussed in the previous sections, the $\mathcal{F}$-statistic becomes singular in the limit $T_{\mathrm{seg}} \to 0$ for single-detector segments due to failure of the maximum-likelihood estimation for all four amplitude parameters $\mathcal{A}^\mu$ that describe the full "+" and "×" polarization content of the CW. These four amplitudes translate into $\nu = 4$ degrees of freedom of the resulting χ^2 distribution governing the $\mathcal{F}$-statistic.

These considerations suggest a strategy for avoiding degeneracy by reducing the number of amplitude parameters (i.e., degrees of freedom) we try to infer about the signal: even with a single stationary detector, *two* amplitudes should always be perfectly well determined, namely, those corresponding to the "+" polarization aligned with the arms of the detector. In the $\mathcal{F}$-statistic framework, the two antenna-pattern functions $a(t)$ and $b(t)$ represent the responses to the two gravitational wave polarizations projected on a sky-position dependent coordinate frame [12].

Guided by this intuition, we construct a new detection statistic by selecting the "dominant response" between a

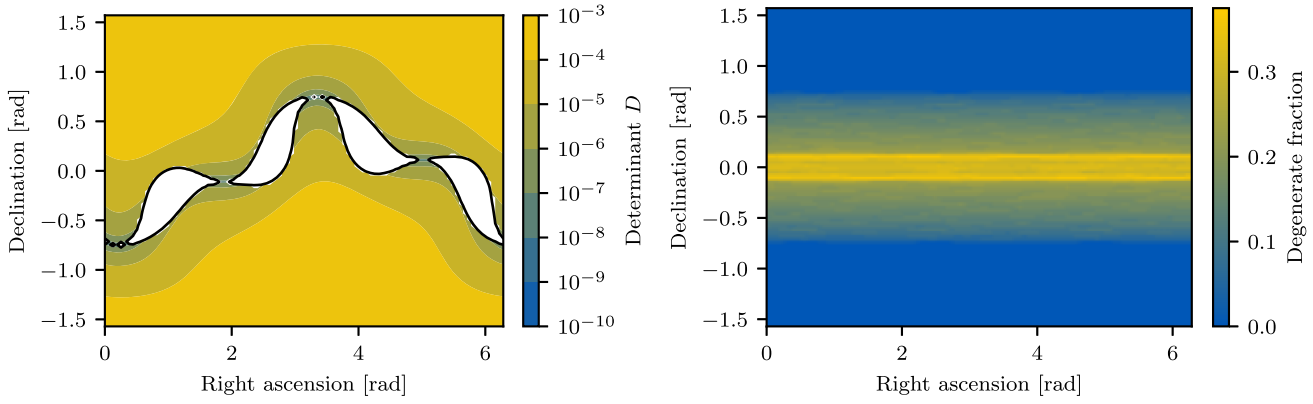

FIG. 1. Antenna-pattern degeneracy for a single detector (H1) and short segments of $T_{\mathrm{seg}} = 900$ s. Left plot: block determinant D over the sky for a single segment. Contour lines mark the region where $\mathcal{M}$ is considered numerically ill conditioned, i.e., $\mathrm{cond}[\mathcal{M}] > 10^4$. Right plot: fraction of segments with ill conditioned antenna-pattern matrix as a function of sky position, using $N_{\mathrm{seg}} = 96$ segments.

and b in each sky position. In other words, we implicitly use only two well-determined amplitude parameters and neglect the other two, effectively reducing the χ^2 degrees of freedom of the resulting statistic to $\nu = 2$.[2]

An interesting alternative construction (described in the Appendix) consists in completely neglecting the antenna-pattern response, resulting in a pure "demodulated power" statistic. While this works for a single detector, it does not generalize well to multiple detectors (suffering destructive interference), contrary to the dominant-response statistic introduced here.

1. The dominant-response $\mathcal{F}_{\mathrm{AB}}$-statistic

Let us consider the special case $b(t) = 0$, which implies $B = C = 0$, $h_2 = h_4 = 0$, and further $x_2 = x_4 = 0$, such that the likelihood Eq. (4) reduces to

$$\ln \mathcal{L}_{\mathrm{A}} = \mathcal{A}^1 x_1 + \mathcal{A}^3 x_3 - \frac{1}{2}\gamma A[(\mathcal{A}^1)^2 + (\mathcal{A}^3)^2]. \tag{26}$$

Maximization over the remaining two amplitude coordinates $\mathcal{A}^1$ and $\mathcal{A}^3$ yields

$$2\mathcal{F}_{\mathrm{A}} = \frac{x_1^2 + x_3^2}{\gamma A}. \tag{27}$$

Similarly, if one had assumed $a(t) = 0$ instead, which implies $x_1 = x_3 = 0$, we would find

$$2\mathcal{F}_{\mathrm{B}} = \frac{x_2^2 + x_4^2}{\gamma B}. \tag{28}$$

Given the noise expectations of Eq. (14), in particular, $E[n_1^2] = E[n_3^2] = \gamma A$ and $E[n_2^2] = E[n_4^2] = \gamma B$, we see that the two statistics $\mathcal{F}_{\mathrm{A}}, \mathcal{F}_{\mathrm{B}}$ are squared sums of Gaussian unit-variance variables; therefore, they are χ^2 distributed with $\nu = 2$ degrees of freedom. The corresponding noncentrality parameters $\rho_{\mathrm{A}}^2, \rho_{\mathrm{B}}^2$, namely,

$$E[2\mathcal{F}_{\mathrm{A}}] = 2 + \rho_{\mathrm{A}}^2, \qquad E[2\mathcal{F}_{\mathrm{B}}] = 2 + \rho_{\mathrm{B}}^2, \tag{29}$$

can be expressed explicitly as

$$\begin{aligned} \rho_{\mathrm{A}}^2 &= \frac{s_1^2 + s_3^2}{\gamma A} = h_0^2\gamma\left[\alpha_1 A + \alpha_2 \frac{C^2}{A} + 2\alpha_3 C\right], \\ \rho_{\mathrm{B}}^2 &= \frac{s_2^2 + s_4^2}{\gamma B} = h_0^2\gamma\left[\alpha_1 \frac{C^2}{B} + \alpha_2 B + 2\alpha_3 C\right]. \end{aligned} \tag{30}$$

Note that the *only* difference to the $\mathcal{F}$-statistic noncentrality ρ^2 of Eq. (20) is the replacement of $B \mapsto C^2/A$ in ρ_{A}^2 and $A \mapsto C^2/B$ in ρ_{B}^2. Given that $\mathcal{M}$ is a positive-definite matrix, i.e., $D \equiv AB - C^2 > 0$ and $\alpha_1, \alpha_2 > 0$, this implies that $\{\rho_{\mathrm{A}}^2, \rho_{\mathrm{B}}^2\} < \rho^2$; i.e., unsurprisingly the "signal power" in the statistic is reduced by neglecting one of the two antenna responses. Further note that $C^2/A = B - D/A$ and $C^2/B = A - D/B$, and therefore,

$$\begin{aligned} \rho_{\mathrm{A}}^2 &= \rho^2 - h_0^2\gamma\alpha_2\frac{D}{A}, \\ \rho_{\mathrm{B}}^2 &= \rho^2 - h_0^2\gamma\alpha_1\frac{D}{B}. \end{aligned} \tag{31}$$

We see that both $\rho_{\mathrm{A}}^2, \rho_{\mathrm{B}}^2$ approach ρ^2 as $D \to 0$, so the more degenerate the antenna-pattern matrix is, the less signal power is lost. Following Eq. (22), we can obtain the $\cos\iota, \psi$-averaged noncentrality parameters as

$$\begin{aligned} \langle\rho_{\mathrm{A}}^2\rangle_{\cos\iota,\psi} &= \langle\rho^2\rangle_{\cos\iota,\psi} - \frac{2}{5}h_0^2\gamma\frac{D}{A}, \\ \langle\rho_{\mathrm{B}}^2\rangle_{\cos\iota,\psi} &= \langle\rho^2\rangle_{\cos\iota,\psi} - \frac{2}{5}h_0^2\gamma\frac{D}{B}. \end{aligned} \tag{32}$$

Given that the sensitivity of $\mathcal{F}_{\mathrm{A}}$ and $\mathcal{F}_{\mathrm{B}}$ is determined by the respective noncentrality parameters, this suggests the following practical construction for an $\mathcal{F}$-statistic *fallback* on degenerate segments: use either $\mathcal{F}_{\mathrm{A}}$ or $\mathcal{F}_{\mathrm{B}}$ depending on which of $\langle\rho_{\mathrm{A}}^2\rangle$ or $\langle\rho_{\mathrm{B}}^2\rangle$ dominates for the current sky position, which only depends on the ordering of A and B. We therefore define the *dominant-response* statistic $\mathcal{F}_{\mathrm{AB}}$ as

$$\mathcal{F}_{\mathrm{AB}} \equiv \begin{cases} \mathcal{F}_{\mathrm{A}} & \text{if } A > B, \\ \mathcal{F}_{\mathrm{B}} & \text{otherwise}, \end{cases} \tag{33}$$

with the corresponding noncentrality parameter given by $\rho_{\mathrm{AB}}^2 = \{\rho_{\mathrm{A}}^2 \text{ if } A > B \text{ else } \rho_{\mathrm{B}}^2\}$.

2. Semicoherent generalization $\hat{\mathcal{F}}_{\mathrm{AB}}$

The coherent dominant-response statistic $\mathcal{F}_{\mathrm{AB}}$ defined in the previous section can be summed semicoherently in the same way as the standard $\mathcal{F}$-statistic; i.e., following Eq. (23), we define

$$\hat{\mathcal{F}}_{\mathrm{AB}} \equiv \sum_{\ell=1}^{N_{\mathrm{seg}}} \mathcal{F}_{\mathrm{AB},\ell}, \tag{34}$$

which is χ^2 distributed with $\hat{\nu}_{\mathrm{AB}} = 2N_{\mathrm{seg}}$ degrees of freedom and noncentrality parameter $\hat{\rho}_{\mathrm{AB}}^2$ given by

$$\hat{\rho}_{\mathrm{AB}}^2 = \sum_{\ell} \rho_{\mathrm{AB},\ell}^2. \tag{35}$$

The dominant-response $\mathcal{F}_{\mathrm{AB}}$-statistic can be semicoherently combined with the standard $\mathcal{F}$-statistic on a

[2]A somewhat-related $\nu = 2$ degrees of freedom variant is the $\mathcal{G}$-statistic [18], which assumes that the two amplitude parameters $\cos\iota$ and ψ are *known* from observations for a given pulsar.

per-segment basis, for example, switching to $\mathcal{F}_{\mathrm{AB}}$ whenever D becomes too small in a segment. The resulting "hybrid" semicoherent $\hat{\mathcal{F}}'$-statistic would be χ^2 distributed with $\hat{\nu}' = 4N_4 + 2N_2$ degrees of freedom, where N_ν is the number of segments using the χ^2_ν statistic, such that $N_4 + N_2 = N_{\mathrm{seg}}$. The corresponding noncentrality parameter $\hat{\rho}'^2$ would be the sum of per-segment ρ^2 and ρ^2_{AB} depending on the statistic used in a given segment.

IV. SURPASSING THE $\hat{\mathcal{F}}$-STATISTIC SENSITIVITY

The new *dominant-response* $\hat{\mathcal{F}}_{\mathrm{AB}}$-statistic of the previous section was constructed as a "fallback" for the $\hat{\mathcal{F}}$-statistic in the degenerate limit of an ill-conditioned antenna-pattern matrix $\mathcal{M}$. As we saw in Eq. (30), the corresponding noncentrality parameter ρ^2_{AB} of $\mathcal{F}_{\mathrm{AB}}$ tends toward the $\mathcal{F}$-statistic signal power ρ^2 in the limit of $D \to 0$. However, $\hat{\mathcal{F}}_{\mathrm{AB}}$ only has *two* degrees of freedom per segment instead of the *four* for the standard $\hat{\mathcal{F}}$-statistic. Fewer degrees of freedom means a lower detection threshold at a given false-alarm probability, which implies that there exists a range of nonzero D values for which $\hat{\mathcal{F}}_{\mathrm{AB}}$ will be *more sensitive* than the $\hat{\mathcal{F}}$-statistic, even when the $\hat{\mathcal{F}}$-statistic is still perfectly well defined and numerically stable.[3]

A. Estimating the maximal sensitivity gain

We characterize the sensitivity [7,19] of a statistic $\mathfrak{s}$ by the smallest required "upper limit" signal amplitude $h_0^* = h_{0,p_{\mathrm{fa}}}^{p_{\mathrm{det}}}$ for a population of signals to reach a certain detection probability p_{det} at a given false-alarm probability p_{fa}. These probabilities are defined as

$$p_{\mathrm{fa}} \equiv \int_{\mathfrak{s}_{\mathrm{fa}}}^{\infty} P(\mathfrak{s}|h_0 = 0)\, d\mathfrak{s}, \tag{36}$$

$$p_{\mathrm{det}} \equiv \int_{\mathfrak{s}_{\mathrm{fa}}}^{\infty} P(\mathfrak{s}|h_0 = h_0^*)\, d\mathfrak{s}, \tag{37}$$

where $\mathfrak{s}_{\mathrm{fa}}$ denotes the detection threshold at the given false-alarm probability p_{fa}.

One can obtain an analytic estimate for the critical signal amplitude h_0^* in the limit of a large number of segments $N_{\mathrm{seg}} \gg 1$, where the $\chi^2_{\hat{\nu}}$ distributions tend toward Gaussians with the same mean and standard deviation. Following [4,19,20], we define the rescaled false-alarm threshold as

$$\alpha \equiv \frac{\mathfrak{s}_{\mathrm{fa}} - \hat{\nu}}{2\sqrt{\hat{\nu}}}. \tag{38}$$

[3]This is another illustration that the $\mathcal{F}$-statistic is not optimal, as first shown in [11].

Using the Gaussian approximation, we can solve Eq. (36) for

$$\alpha = \mathrm{erfc}^{-1}(2p_{\mathrm{fa}}), \tag{39}$$

in terms of the inverse of the complementary error function $\mathrm{erfc}(x)$. Similarly, we define

$$\beta \equiv -\mathrm{erfc}^{-1}(2p_{\mathrm{det}}), \tag{40}$$

which is a monotonically increasing function of p_{det} with $\beta > 0$ for $p_{\mathrm{det}} > 0.5$. Further assuming a signal population of fixed power $\hat{\rho}^2$ (instead of fixed amplitude h_0), we can express Eq. (37) as

$$\beta = \frac{\hat{\rho}^2 - 2\alpha\sqrt{\hat{\nu}}}{2\sqrt{\hat{\nu} + 2\hat{\rho}^2}}. \tag{41}$$

For a given $\alpha(p_{\mathrm{fa}})$ and $\beta(p_{\mathrm{det}})$, we can solve this for the critical signal power as

$$\hat{\rho}^2_*(p_{\mathrm{fa}}, p_{\mathrm{det}}) = 2\alpha\sqrt{\hat{\nu}} + 4\beta^2(1 + \sqrt{1 + Q}), \tag{42}$$

with $Q \equiv (\hat{\nu} + 4\alpha\sqrt{\hat{\nu}})/(4\beta^2)$. As shown in [19], this approximation produces a biased estimate for the critical signal amplitude $h_{0,p_{\mathrm{fa}}}^{p_{\mathrm{det}}}$, but we can use it to analyze the *scaling* of sensitivity with search parameters.

We can use Eq. (38) to express the respective detection thresholds in the large-N_{seg} limit as

$$\frac{\hat{\mathcal{F}}_{\mathrm{fa}}}{\hat{\mathcal{F}}_{\mathrm{AB\,fa}}} = \frac{\hat{\nu} + 2\alpha\sqrt{\hat{\nu}}}{\hat{\nu}_{\mathrm{AB}} + 2\alpha\sqrt{\hat{\nu}_{\mathrm{AB}}}} \overset{N_{\mathrm{seg}} \gg 1}{\longrightarrow} \frac{\hat{\nu}}{\hat{\nu}_{\mathrm{AB}}} = 2, \tag{43}$$

while the critical signal power of Eq. (42) tends to

$$\hat{\rho}^2_* \overset{N_{\mathrm{seg}} \gg 1}{\longrightarrow} 2(\alpha + \beta)\sqrt{\hat{\nu}}. \tag{44}$$

Halving the degrees of freedom from $\hat{\nu} = 4N_{\mathrm{seg}}$ for the standard $\mathcal{F}$-statistic to $\hat{\nu}_{\mathrm{AB}} = 2N_{\mathrm{seg}}$ for the dominant-response statistic $\mathcal{F}_{\mathrm{AB}}$ therefore results in a maximal sensitivity gain of

$$\frac{h^*_{0,\mathcal{F}}}{h^*_{0,\mathcal{F}_{\mathrm{AB}}}} \sim \frac{\hat{\rho}_{*,\mathcal{F}}}{\hat{\rho}_{*,\mathcal{F}_{\mathrm{AB}}}} \overset{N_{\mathrm{seg}} \gg 1}{\longrightarrow} \left(\frac{\hat{\nu}}{\hat{\nu}_{\mathrm{AB}}}\right)^{1/4} = 2^{1/4}, \tag{45}$$

i.e., a gain of up to $\approx 18.9\%$ compared to the standard $\mathcal{F}$-statistic.

Note that in this derivation, we assumed $\hat{\rho}^2_{\mathrm{AB}} \approx \hat{\rho}^2$, i.e., $D \approx 0$ in Eq. (31); therefore, the maximal sensitivity gain would decrease when D increases, such as when using longer segments or more detectors.

B. The optimal choice between $\hat{\mathcal{F}}$ and $\hat{\mathcal{F}}_{\mathrm{AB}}$

We have seen in the previous section that when there is no loss in noncentrality, i.e., $\hat{\rho}^2_{\mathrm{AB}} \approx \hat{\rho}^2$, the halving of the χ^2 degrees of freedom results in up to 18.9% sensitivity gain in the large-N_{seg} limit. This argument suggests there should be a critical level of noncentrality loss below which $\hat{\mathcal{F}}_{\mathrm{AB}}$ is more sensitive than $\hat{\mathcal{F}}$.

In order to estimate this transition, we use Eq. (44) to express $\beta = \hat{\rho}^2/\sqrt{\hat{\nu}} - 2\alpha$, where β is a monotonic function of detection probability p_{det}. Therefore the more sensitive statistic is characterized by a higher $\hat{\rho}^2/\sqrt{\hat{\nu}}$. This can be reformulated into the condition

$$\hat{\mu}_{\mathrm{AB}} \equiv \frac{\hat{\rho}^2 - \hat{\rho}^2_{\mathrm{AB}}}{\hat{\rho}^2} < \frac{\sqrt{2}-1}{\sqrt{2}} \approx 0.29, \tag{46}$$

in terms of the *noncentrality mismatch* $\hat{\mu}_{\mathrm{AB}}$. Therefore, up to a loss of $\hat{\mu}_{\mathrm{AB}} \lesssim 29\%$ in noncentrality, there is still a net sensitivity gain for the dominant-response statistic $\hat{\mathcal{F}}_{\mathrm{AB}}$ due to the reduction in degrees of freedom.

This condition is not practically usable as it depends on the unknown signal amplitude parameters $\cos\iota$ and ψ, but we can use the averages of Eq. (32) to obtain an estimate

$$\hat{m}_{\mathrm{AB}} \equiv \langle \mu_{\mathrm{AB}} \rangle_{\cos\iota,\psi} \sim \frac{\sum_\ell \frac{D_\ell}{\max(A,B)_\ell}}{\sum_\ell (A_\ell + B_\ell)}, \tag{47}$$

where we approximated the average of the fraction as the fraction of averages, which is generally biased but numerically turns out to be a relatively good approximation in this case. Therefore, we expect the dominant-response $\mathcal{F}_{\mathrm{AB}}$-statistic to be more sensitive than the $\mathcal{F}$-statistic when

$$\hat{m}_{\mathrm{AB}} \lesssim 0.29. \tag{48}$$

For sufficiently short segments, this criterion will be satisfied essentially over the whole sky, favoring $\hat{\mathcal{F}}_{\mathrm{AB}}$, while for long-enough segments it will not be satisfied anywhere, favoring $\hat{\mathcal{F}}$, with an intermediate regime of segment lengths where the optimal choice will depend on the sky position.

V. NUMERICAL RESULTS

In this section, we numerically test the theoretical predictions derived in the previous sections and further characterize the performance of the new statistic $\hat{\mathcal{F}}_{\mathrm{AB}}$. We use two complementary numerical methods for sensitivity estimation in order to cross-check and validate the implementations and results:

(1) Direct numerical integration of the known χ^2 distributions for the two statistics $\hat{\mathcal{F}}$ and $\hat{\mathcal{F}}_{\mathrm{AB}}$, using the explicit noncentrality expressions for $\hat{\rho}^2$ and $\hat{\rho}^2_{\mathrm{AB}}$ given in Eqs. (20) and (30), respectively. This is essentially the sensitivity-estimation method described in [7,19].

(2) Sampling *synthesized* statistic values (per segment) by drawing noise-realizations for the four Gaussian variates n_μ with covariance matrix $\mathcal{M}_{\mu\nu}$ of Eq. (14) and adding signal contributions $s_\mu = \mathcal{M}_{\mu\nu}\mathcal{A}^\nu$ for $\mathcal{A}^\mu$ drawn from their priors. Both the standard $\mathcal{F}$-statistic as well as $\mathcal{F}_{\mathrm{AB}}$ are fully determined by the four numbers $x_\mu = n_\mu + s_\mu$, as seen in Eq. (17) and Eqs. (27), (28), respectively. This synthetic sampling method has been used previously in [11,21].

Both these methods are substantially faster than full injection-and-recovery simulations and "cleaner" in the sense of not being affected by noise-estimation biases and intrinsic implementation losses when computing $\hat{\mathcal{F}}$-statistics on actual data. Therefore, these methods allow us to explore larger parameter spaces and characterize the intrinsic properties of these statistics. Compared to direct integration, sampling of synthetic statistic values is more limited due to the finite number of samples generated in a given amount of time, resulting in lower accuracy and limitations on how small false-alarm probabilities p_{fa} can be simulated.

For these tests, we assume perfect Gaussian noise and data without gaps. For the sake of example, sensitivity is characterized at an "upper limit" confidence level of $p_{\mathrm{det}} = 90\%$ and for a *single-template* false-alarm level of $p_{\mathrm{fa}} = 10^{-10}$. This choice would correspond to an overall false-alarm level of $\sim 1\%$ over a parameter-space region containing $\sim 10^8$ (independent) templates, which would be a reasonably realistic choice for typical wide-parameter-space searches.

The sensitivity of a search can be conveniently characterized by its *sensitivity depth* [7,22], defined as

$$\mathcal{D}^{p_{\mathrm{det}}}_{p_{\mathrm{fa}}} \equiv \frac{\sqrt{\mathcal{S}}}{h^{p_{\mathrm{det}}}_{0,p_{\mathrm{fa}}}}, \tag{49}$$

in terms of the overall noise power spectral density $\mathcal{S}$ of Eq. (7) and the sensitivity amplitude $h^{p_{\mathrm{det}}}_{0,p_{\mathrm{fa}}}$ introduced in Sec. IV A. This definition scales out the noise-floor dependence and better characterizes the intrinsic method sensitivity.

A. Example: Segments of $T_{\mathrm{seg}} = 900$ s over 6 months

We consider the following example setup[4] to illustrate the performance of the dominant-response statistic $\hat{\mathcal{F}}_{\mathrm{AB}}$ compared to the standard $\hat{\mathcal{F}}$-statistic: an all-sky search on 6 months of data without gaps using $N_{\mathrm{seg}} = 17\,280$ segments of length $T_{\mathrm{seg}} = 900$ s.

[4]Based on a recent all-sky binary search [8] on O3a data, which used $N_{\mathrm{seg}} = 16\,966$ segments (with gaps) of $T_{\mathrm{seg}} = 900$ s.

TABLE I. Sensitivity depth $\mathcal{D}$ (in units of $1/\sqrt{\text{Hz}}$) for the standard $\hat{\mathcal{F}}$-statistic and the dominant-response $\hat{\mathcal{F}}_{\text{AB}}$-statistic at $p_{\text{fa}} = 10^{-10}$ and $p_{\text{det}} = 90\%$. The search setup consists of $N_{\text{seg}} = 17\,280$ segments of $T_{\text{seg}} = 900$ s, for different sets of detectors.

Detectors	$\mathcal{D}(\hat{\mathcal{F}})$	$\mathcal{D}(\hat{\mathcal{F}}_{\text{AB}})$	Gain (%)
H1	18.3	21.7	18.6
H1, L1	26.3	30.5	16.2
H1, L1, V1	32.1	35.0	9.0

The detection thresholds for the two statistics are found as $\hat{\mathcal{F}}_{\text{fa}} \approx 6.4 \times 10^4$ and $\hat{\mathcal{F}}_{\text{ABfa}} \approx 3.3 \times 10^4$, with a ratio of ≈ 1.97, very close to the theoretical prediction of Eq. (43).

We can numerically estimate the sensitivity depths for the two statistics as shown in Table I, for one (H1), two (H1 + L1), or three detectors (H1 + L1 + V1). We see that for a single detector the sensitivity gain of $\hat{\mathcal{F}}_{\text{AB}}$ versus $\hat{\mathcal{F}}$ is close to the theoretical maximum of 18.9%, while increasing the number of detectors reduces the gain, down to about 9% for three detectors. This behavior stems from the short-segment antenna pattern being more degenerate for a single detector (i.e., D is closer to zero), keeping the noncentrality loss of $\hat{\rho}^2_{\text{AB}}$ versus $\hat{\rho}^2$ small, while using more detectors reduces the degeneracy and thereby increases the mismatch $\hat{m}_{\text{AB}}$.

Figure 2 shows the receiver-operator characteristic, i.e., p_{det} versus p_{fa}, for two detectors (H1 + L1) and signals at fixed depth $\mathcal{D}^{90\%}_{10^{-10}}(\hat{\mathcal{F}})$ of Table I. At the false-alarm level of $p_{\text{fa}} = 10^{-10}$, the detection probability of the dominant-response statistic $\hat{\mathcal{F}}_{\text{AB}}$ is about 8% higher than that of the $\hat{\mathcal{F}}$-statistic. Figure 3 shows the *efficiency curve*, i.e., p_{det} versus signal strength quantified in terms of the depth $\mathcal{D}$.

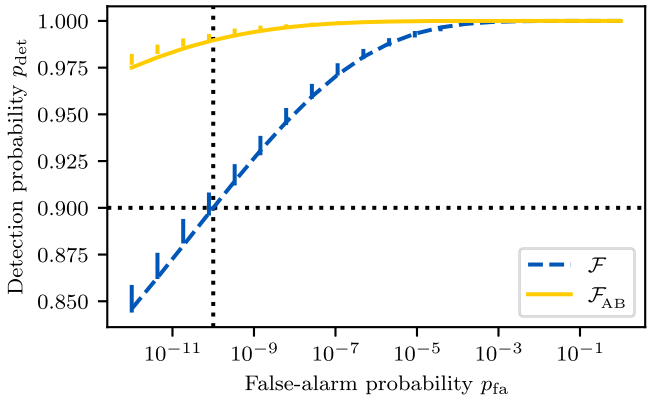

FIG. 2. Receiver-operator characteristic for the dominant-response $\hat{\mathcal{F}}_{\text{AB}}$-statistic and the standard $\hat{\mathcal{F}}$-statistic, on a signal population of fixed depth $\mathcal{D}^{90\%}_{10^{-10}}(\hat{\mathcal{F}})$, using two different numerical methods: direct integration (solid lines) and synthetic statistic sampling (error bars showing 90% confidence regions). The search setup consists of $N_{\text{seg}} = 17\,280$ segments of $T_{\text{seg}} = 900$ s for two detectors (H1 + L1).

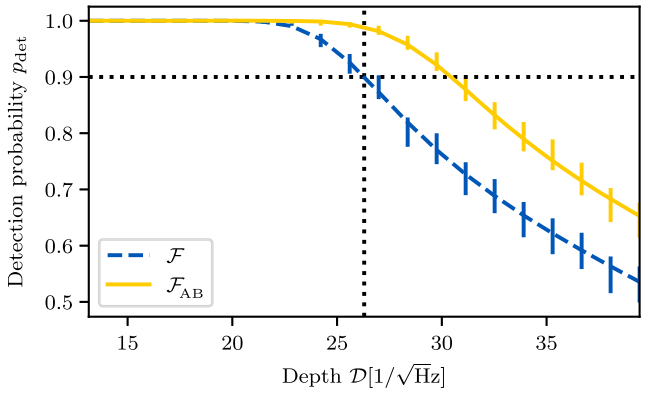

FIG. 3. Efficiency curves for the dominant-response $\hat{\mathcal{F}}_{\text{AB}}$-statistic and the standard $\hat{\mathcal{F}}$-statistic, at a (single-template) false-alarm level of $p_{\text{fa}} = 10^{-10}$, using two different numerical methods: direct integration (solid lines) and synthetic statistic sampling (error bars showing 90% confidence regions). The search setup consists of $N_{\text{seg}} = 17\,280$ segments of $T_{\text{seg}} = 900$ s for two detectors (H1 + L1).

B. Sensitivity gain versus segment length T_{seg}

An interesting question of practical importance is up to which "critical" segment length T^*_{seg} the dominant-response $\hat{\mathcal{F}}_{\text{AB}}$-statistic performs better than the $\hat{\mathcal{F}}$-statistic. The answer to this question is shown in Fig. 4 for a two-detector (H1 + L1) all-sky search. We see that the transition point is at about $T^*_{\text{seg}} \sim 20\,000$ s, very similar to the H1-only case (not shown here), while adding Virgo (H1 + L1 + V1) would bring this down to about $T^*_{\text{seg}} \sim 15\,000$ s (not shown here).

The underlying reason for the decreasing gains of $\hat{\mathcal{F}}_{\text{AB}}$ lies in the increasing noncentrality mismatch $\hat{m}_{\text{AB}}$, which will also depend on the sky position. Therefore, searches

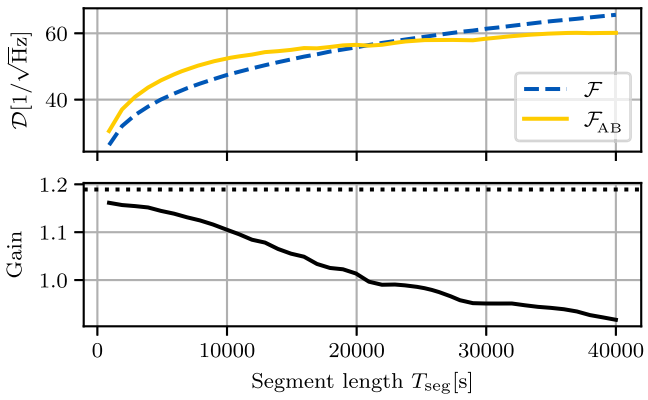

FIG. 4. Sensitivity depth $\mathcal{D}^{90\%}_{10^{-10}}$ and relative sensitivity gain as a function of segment length T_{seg} for the dominant-response $\hat{\mathcal{F}}_{\text{AB}}$-statistic versus the standard $\hat{\mathcal{F}}$-statistic. The dotted horizontal line indicates the theoretical maximal sensitivity gain of 8.9%. The search setup spans 6 months using two detectors (H1 + L1).

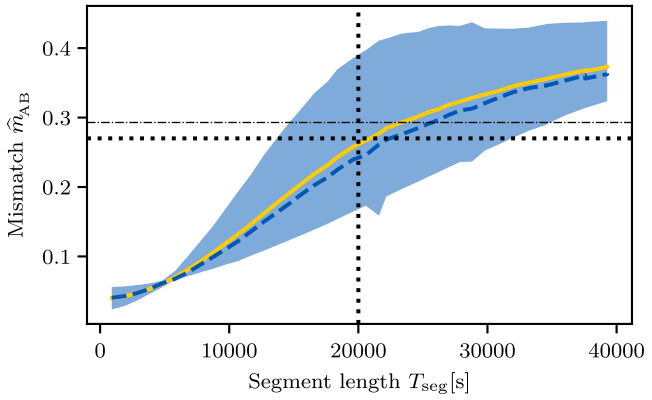

FIG. 5. Distribution (over the sky) of the noncentrality mismatch $\hat{m}_{\mathrm{AB}}$ as a function of segment length T_{seg} for a two-detector search setup (H1 + L1). The solid line indicates the mean mismatch, the dashed line the median, and the band the range from the 10th to the 90th percentile. The horizontal dotted-dashed line corresponds to the theoretical estimate $\hat{m}^*_{\mathrm{AB}} \approx 0.29$ of Eq. (48) for the critical mismatch, while the dotted vertical line indicates the observed transition segment length $T^*_{\mathrm{seg}} \sim 20\,000$ s of Fig. 4. The resulting *empirical* estimate for the critical mismatch is $\hat{m}^*_{\mathrm{AB}} \sim 0.27$ (dotted horizontal line).

directed at a single sky position will have different transition segment lengths dependent on that sky position.

To partially address this question, in Fig. 5, we plot the mismatch distribution (for H1 + L1) versus segment length. This shows that, somewhat consistently with Fig. 4 and the theoretical estimate Eq. (48), the mean noncentrality mismatch crosses the theoretical estimate of the "critical" mismatch of $\hat{m}^*_{\mathrm{AB}} \sim 0.29$ (dashed horizontal line) at about $T_{\mathrm{seg}} \sim 22\,000$ s, while at the observed critical segment length of $T_{\mathrm{seg}} \sim 20\,000$ s in Fig. 5 the corresponding *empirical* critical mismatch would be about

$$\hat{m}^*_{\mathrm{AB}} \sim 0.27. \tag{50}$$

From this plot, we would also predict $\hat{\mathcal{F}}_{\mathrm{AB}}$ to be more sensitive in every sky position below $T_{\mathrm{seg}} \lesssim 15\,000$ s, while $\hat{\mathcal{F}}$ should be more sensitive in every sky position above $T_{\mathrm{seg}} \gtrsim 35\,000$ s. For intermediate segment lengths, the choice of the optimal statistic will be a function of the sky position.

C. Sensitivity gain versus mismatch $\hat{m}_{\mathrm{AB}}$

From earlier theoretical considerations in Sec. IV B as well as the empirical results in the previous section, we expect the noncentrality mismatch $\hat{m}_{\mathrm{AB}}$ to be the intrinsic factor determining the gain of $\hat{\mathcal{F}}_{\mathrm{AB}}$ versus $\hat{\mathcal{F}}$. This mismatch is a function not only of the segment setup and detectors but also of the sky position, as illustrated in Fig. 6. Here, we see the noncentrality mismatch for a two-detector (H1 + L1) setup over one day (the antenna patterns are periodic over a day) for two different segment lengths, $T_{\mathrm{seg}} = 900$ s and $T_{\mathrm{seg}} = 17\,100$ s. This example illustrates that the mismatch can be highest at the poles or the equator, depending on the detailed setup (detectors, segment lengths), and increases for longer segments.

Following the discussion in Sec. IV B and especially Eq. (48), we expect the critical mismatch value to be around $\hat{m}^*_{\mathrm{AB}} \approx 0.29$, while empirical results in Fig. 5 and Eq. (50) suggest a slightly lower critical value of about $\hat{m}_{\mathrm{AB}} \sim 0.27$.

We can test these predictions by plotting the sensitivity gain as a function of noncentrality mismatch $\hat{m}_{\mathrm{AB}}$ (by varying the sky position), where we chose an example near the transition, namely, $T_{\mathrm{seg}} = 17\,100$ s. The result is shown in Fig. 7, for a two-detector setup (H1 + L1) and a 6 months total observation span. These results confirm that indeed the sensitivity gain correlates strongly with the noncentrality mismatch and that the transition does happen close to the theoretically predicted value, albeit with the empirical prediction of $\hat{m}^*_{\mathrm{AB}} \sim 0.27$ being closer to the truth.

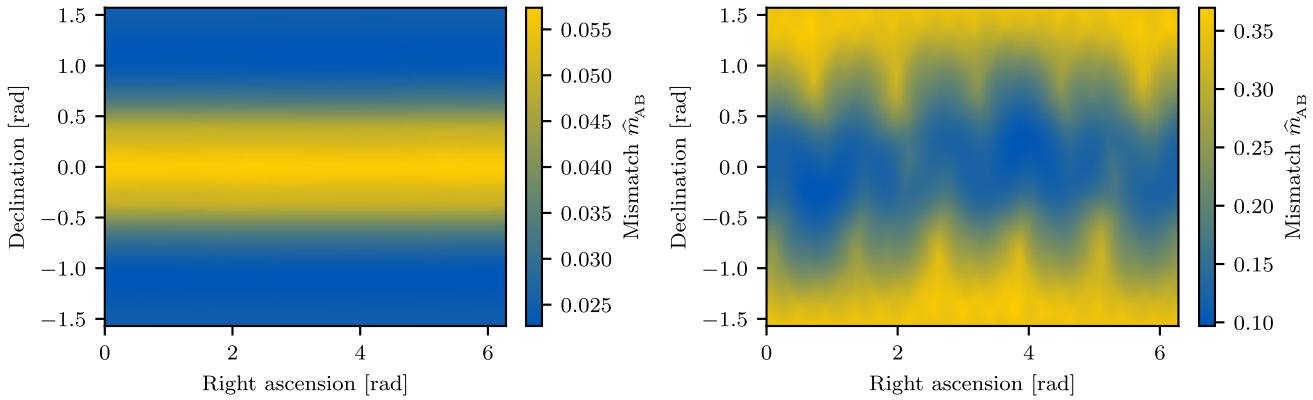

FIG. 6. Noncentrality mismatch $\hat{m}_{\mathrm{AB}}$ as a function of sky position for a two-detector search setup (H1 + L1) spanning one day, using $N_{\mathrm{seg}} = 96$ segments of $T_{\mathrm{seg}} = 900$ s duration (left plot) and $N_{\mathrm{seg}} = 6$ segments of $T_{\mathrm{seg}} = 17\,100$ s duration (right plot).

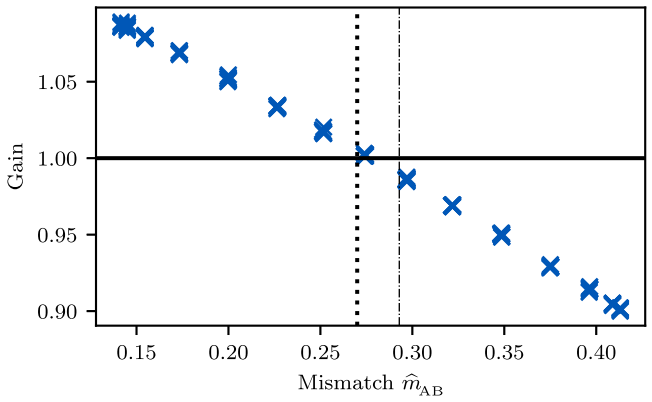

FIG. 7. Sensitivity gain of the dominant-response $\hat{\mathcal{F}}_{\mathrm{AB}}$-statistic over the standard $\hat{\mathcal{F}}$-statistic for single-sky-position searches as a function of the corresponding noncentrality mismatch $\hat{m}_{\mathrm{AB}}$ in the sky position. The vertical dotted-dashed line corresponds to the theoretical estimate $\hat{m}^*_{\mathrm{AB}} \approx 0.29$ of Eq. (48), while the vertical dotted line indicates the empirical critical mismatch of $\hat{m}^*_{\mathrm{AB}} \sim 0.27$ estimated in Fig. 5. The search setup consists of $N_{\mathrm{seg}} = 910$ segments of $T_{\mathrm{seg}} = 17\,100$ s duration using two detectors (H1 + L1).

VI. CONCLUSIONS

In this paper, we have shown that the standard $\mathcal{F}$-statistic becomes singular for very short segments due to the degeneracy of the antenna-pattern matrix. This observation lead us to construct a well-behaved "fallback" statistic, referred to as the *dominant-response* $\mathcal{F}_{\mathrm{AB}}$-statistic. Somewhat surprisingly, however, this new statistic turns out to be *more sensitive* than the $\mathcal{F}$-statistic by up to $\approx$19%, even outside the degeneracy region of the $\mathcal{F}$-statistic, when semicoherently combining a large number of short segments. We have characterized the new $\mathcal{F}_{\mathrm{AB}}$-statistic analytically and numerically and shown that it is more sensitive than the $\mathcal{F}$-statistic for segments shorter than $T_{\mathrm{seg}} \lesssim 15\,000$ s to 20 000 s (depending on the number of detectors used).

We have further shown that the sensitivity gain is determined by the noncentrality mismatch $\hat{m}_{\mathrm{AB}}$ of Eq. (47), and theoretical and empirical estimates place the transition at about $\hat{m}_{\mathrm{AB}} \sim 0.27$, below which $\mathcal{F}_{\mathrm{AB}}$ is more sensitive than $\mathcal{F}$.

The new detection statistic uses the same signal phase model as the $\mathcal{F}$-statistic and is therefore expected [10] to require essentially the same number of templates and computing cost for a given parameter space.

Future work will focus on reanalyzing this limit in a Bayesian framework following the approach of [11].

ACKNOWLEDGMENTS

We thank David Keitel for helpful feedback. This work has utilized the ATLAS computing cluster at the MPI for Gravitational Physics Hannover.

APPENDIX: CONSTANT-RESPONSE STATISTIC $\mathcal{F}_\phi$

As an alternative construction to the dominant-response statistic $\mathcal{F}_{\mathrm{AB}}$ introduced in Sec. III B 1, it is interesting to consider another special case obtained by assuming a constant amplitude response, i.e., completely neglecting the antenna-pattern modulation, and define a template,

$$\begin{aligned} h^X_\phi(t) &= \mathcal{A}\cos(\phi^X(t) + \phi_0) \\ &= \mathcal{A}_{\mathrm{c}}\cos\phi^X(t) + \mathcal{A}_{\mathrm{s}}\sin\phi^X(t), \end{aligned} \tag{A1}$$

where $\mathcal{A}_{\mathrm{c}} \equiv \mathcal{A}\sin\phi_0$ and $\mathcal{A}_{\mathrm{s}} \equiv \mathcal{A}\cos\phi_0$. Using this template family, the log-likelihood of Eq. (4) takes the form

$$\ln\mathcal{L} = \mathcal{A}_{\mathrm{s}}x_{\mathrm{s}} + \mathcal{A}_{\mathrm{c}}x_{\mathrm{c}} - \frac{\gamma}{2}\mathcal{A}^2, \tag{A2}$$

where we defined

$$x_{\mathrm{c}} \equiv (x|\cos\phi), \qquad x_{\mathrm{s}} \equiv (x|\sin\phi), \tag{A3}$$

in terms of the (multidetector) scalar product $(x|y)$ of Eq. (6). Maximizing this log likelihood over the two unknown amplitudes $\mathcal{A}_{\mathrm{c}}, \mathcal{A}_{\mathrm{s}}$ yields $\mathcal{A}'_{\mathrm{s,c}} = \gamma^{-1}x_{\mathrm{s,c}}$, and substituting back results in the partially maximized likelihood

$$2\mathcal{F}_\phi \equiv 2\ln\mathcal{L}' = \gamma^{-1}(x_{\mathrm{c}}^2 + x_{\mathrm{s}}^2), \tag{A4}$$

defining the *constant-response* $\mathcal{F}_\phi$-statistic. Note that $x_{\mathrm{c}}^2 + x_{\mathrm{s}}^2$ in the single-detector case is precisely the Fourier power of $x(t)$ demodulated into the source frame.

In the short-segment limit $T_{\mathrm{seg}} \to 0$ for a single detector, this would tend exactly to the dominant-response $\mathcal{F}_{\mathrm{AB}}$-statistic, as in this limit $a(t) \to a_0$, $b(t) \to b_0$, and therefore, $A \to a_0^2$, $B \to b_0^2$ and also $x_\mu \to \{a_0, b_0\}x_{\mathrm{s,c}}$.

Similarly to Sec. III B 1, one can show that this statistic follows a χ^2 distribution with $\nu = 2$ degrees of freedom, namely,

$$E[2\mathcal{F}_\phi] = 2 + \rho_\phi^2, \tag{A5}$$

with a noncentrality parameter,

$$\rho_\phi^2 \equiv \gamma^{-1}(s_{\mathrm{c}}^2 + s_{\mathrm{s}}^2), \tag{A6}$$

in terms of the signal projections $s_{\mathrm{s,c}} \equiv (s|\{\sin,\cos\}\phi)$. Using the scalar product of Eq. (6) with the basis functions of Eq. (3), we find

$$\begin{aligned} s_{\mathrm{c}} &= \gamma(\mathcal{A}^1\langle\boldsymbol{a}\rangle + \mathcal{A}^2\langle\boldsymbol{b}\rangle), \\ s_{\mathrm{s}} &= \gamma(\mathcal{A}^3\langle\boldsymbol{a}\rangle + \mathcal{A}^4\langle\boldsymbol{b}\rangle), \end{aligned} \tag{A7}$$

using the noise-weighted multidetector average defined in Eq. (12). Combining this with Eq. (21), we can express the constant-response noncentrality as

$$\rho_\phi^2 = h_0^2\gamma[\alpha_1\langle \boldsymbol{a}\rangle^2 + \alpha_2\langle \boldsymbol{b}\rangle^2 + 2\alpha_3\langle \boldsymbol{a}\rangle\langle \boldsymbol{b}\rangle], \quad \text{(A8)}$$

which has an uncanny formal resemblance to the $\mathcal{F}$-statistic signal power expression of Eq. (20), except that the mean squares of antenna-pattern functions of Eq. (11) are now replaced by squared means, i.e., $\langle \boldsymbol{a}^2\rangle \mapsto \langle \boldsymbol{a}\rangle^2$, $\langle \boldsymbol{b}^2\rangle \mapsto \langle \boldsymbol{b}\rangle^2$ and $\langle \boldsymbol{ab}\rangle \mapsto \langle \boldsymbol{a}\rangle\langle \boldsymbol{b}\rangle$. This observation implies that for a single detector in the short-segment limit, this statistic will again have the same noncentrality as the $\mathcal{F}$-statistic with only half the degrees of freedom, gaining the same $\approx 18.9\%$ in sensitivity as the dominant-response $\mathcal{F}_{\mathrm{AB}}$-statistic of Sec. III B 1.

For longer observation times as well as multiple detectors, however, the antenna-pattern function can cancel out in the averages, resulting in potentially significant sensitivity losses. Especially for nonaligned detectors, the multidetector averages can cancel strongly, potentially making $\mathcal{F}_\phi$ more suitable as a "veto" rather than a detection statistic.

[1] R. Prix, Gravitational waves from spinning neutron stars, in *Neutron Stars and Pulsars*, edited by W. Becker (Springer Berlin Heidelberg, 2016), Vol. 357, Chap. 24, pp. 651–685, 10.1007/978-3-540-76965-1_24.

[2] B. Haskell and K. Schwenzer, Gravitational waves from isolated neutron stars, arXiv:2104.03137.

[3] P. R. Brady and T. Creighton, Searching for periodic sources with LIGO. II. Hierarchical searches, Phys. Rev. D **61**, 082001 (2000).

[4] R. Prix and M. Shaltev, Search for continuous gravitational waves: Optimal stackslide method at fixed computing cost, Phys. Rev. D **85**, 084010 (2012).

[5] P. Jaranowski, A. Królak, and B. F. Schutz, Data analysis of gravitational-wave signals from spinning neutron stars: The signal and its detection, Phys. Rev. D **58**, 063001 (1998).

[6] C. Cutler and B. F. Schutz, Generalized $\mathcal{F}$-statistic: Multiple detectors and multiple gravitational wave pulsars, Phys. Rev. D **72**, 063006 (2005).

[7] C. Dreissigacker, R. Prix, and K. Wette, Fast and accurate sensitivity estimation for continuous-gravitational-wave searches, Phys. Rev. D **98**, 084058 (2018).

[8] P. B. Covas, M. A. Papa, R. Prix, and B. J. Owen, Constraints on r-modes and mountains on millisecond neutron stars in binary systems, Astrophys. J. Lett. **929**, L19 (2022).

[9] R. Prix, The $\mathcal{F}$-statistic and its implementation in ComputeFstatistic_v2, Technical Report No. LIGO-T0900149-v6, 2010, https://dcc.ligo.org/LIGO-T0900149/public.

[10] R. Prix, Search for continuous gravitational waves: Metric of the multidetector $\mathcal{F}$-statistic, Phys. Rev. D **75**, 023004 (2007).

[11] R. Prix and B. Krishnan, Targeted search for continuous gravitational waves: Bayesian versus maximum-likelihood statistics, Classical Quantum Gravity **26**, 204013 (2009).

[12] J. T. Whelan, R. Prix, C. J. Cutler, and J. L. Willis, New coordinates for the amplitude parameter space of continuous gravitational waves, Classical Quantum Gravity **31**, 065002 (2014).

[13] K. Wette, Geometric approach to analytic marginalisation of the likelihood ratio for continuous gravitational wave searches, Universe **7**, 174 (2021).

[14] J. J. Bero and J. T. Whelan, An analytic approximation to the bayesian detection statistic for continuous gravitational waves, Classical Quantum Gravity **36**, 015013 (2019).

[15] J. Ming, B. Krishnan, M. A. Papa, C. Aulbert, and H. Fehrmann, Optimal directed searches for continuous gravitational waves, Phys. Rev. D **93**, 064011 (2016).

[16] J. Ming, M. A. Papa, B. Krishnan, R. Prix, C. Beer, S. J. Zhu, H. B. Eggenstein, O. Bock, and B. Machenschalk, Optimally setting up directed searches for continuous gravitational waves in advanced LIGO O1 data, Phys. Rev. D **97**, 024051 (2018).

[17] LIGO Scientific Collaboration, LIGO Algorithm Library—LALSuite, free software (GPL) (2018), 10.7935/GT1W-FZ16.

[18] P. Jaranowski and A. Królak, Searching for gravitational waves from known pulsars using the $\mathcal{F}$ and $\mathcal{G}$ statistics, Classical Quantum Gravity **27**, 194015 (2010).

[19] K. Wette, Estimating the sensitivity of wide-parameter-space searches for gravitational-wave pulsars, Phys. Rev. D **85**, 042003 (2012).

[20] B. Krishnan, A. M. Sintes, M. A. Papa, B. F. Schutz, S. Frasca, and C. Palomba, Hough transform search for continuous gravitational waves, Phys. Rev. D **70**, 082001 (2004).

[21] D. Keitel, R. Prix, M. A. Papa, P. Leaci, and M. Siddiqi, Search for continuous gravitational waves: Improving robustness versus instrumental artifacts, Phys. Rev. D **89**, 064023 (2014).

[22] B. Behnke, M. Alessandra Papa, and R. Prix, Postprocessing methods used in the search for continuous gravitational-wave signals from the galactic center, Phys. Rev. D **91**, 064007 (2015).